JOURNAL OF THEORETICAL AND APPLIED MECHANICS
49, 4, pp. 1217-1232, Warsaw 2011

NUMERICAL SIMULATION OF TURBULENT HEAT AND MOMENTUM TRANSPORT IN ROTATING CAVITY[1]

Ewa Tuliszka-Sznitko
Wojciech Majchrowski
Kamil Kiełczewski

Pozna University of Technology, Institute of Thermal Engineering, Poznań, Poland
e-mail: ewa.tuliszka-sznitko@put.poznan.pl

The paper gives the results of the Direct Numerical Simulation (DNS) and Large Eddy simulation (LES) which were performed to investigate the 3D transitional non-isothermal flows within a rotor/stator cavity. A Lagrangean version of the dynamic Smagorinsky eddy viscosity model was used. Computations were performed for the cavity of the aspect ratio $L = 3.0\text{-}5.0$, curvature parameters $R_m = 1.8\text{-}5.0$, for the Reynolds number $\mathrm{Re} = (1.0\text{-}2.5) \cdot 10^5$ and for different Prandtl numbers. The results were obtained for coupled momentum and thermal transport in the rotor/stator cavity flows. The obtained distributions of the turbulent heat flux tensor components, the Reynolds stress tensor components, the turbulent Prandtl number and other structural parameters coincide with the experimental data (published in the literature).

Key words: laminar-turbulent transition, rotating cavities, LES, DNS

1. Introduction

The instability structures of the flow in the rotor/stator and rotor/rotor cavity have been investigated since the sixties of the last century, mostly with the reference to applications in turbomachinery. It is also a very interesting fundamental problem: the flow between rotating disks is one of the simplest 3D flows, highly suitable for investigating the influence of mean flow parameters on transitional and turbulence structures. The flow in rotor/stator cavity was investigated experimentally and numerically among others by Andersson and Lygren (2006), Gauthier *et al.* (2002), Moisy *et al.* (2004), Serre and Pulicani (2001), Serre *et al.* (2004), Lygren and Anderson (2004), Séverac

[1]Paper presented at the XIX Polish National Fluid Dynamics Conference

and Serre (2007), Tuliszka-Sznitko *et al.* (2002, 2008, 2009a,b, 2010). Lygren and Anderson (2004) performed the LES of the flow in an open rotor/stator cavity using three different models, and compared the results with those obtained by DNS. Séverac and Serre (2007) performed numerical computations for the enclosed cavity for the Reynolds number up to $\mathrm{Re} = \Omega R_1^2/\nu = 10^6$ ($L = (R_1 - R_0)/2h = 5.0$, $Rm = (R_1 + R_0)/(R_1 - R_0) = 1.8$) using the Spectral Vanishing Viscosity (SVV) method, and compared the results with their LDV experimental data. The non-isothermal flow conditions were also considered in some investigations (Tuliszka-Sznitko *et al.* 2002, 2008, 2009a, 2010; Randriamampianina *et al.*, 1987), which showed that the thermal effects and the rotation-induced buoyancy influence the stability characteristics and the critical conditions. Tuliszka-Sznitko *et al.* (2009a) performed the LES of the non-isothermal flow in the rotor/stator cavity, delivering distributions of the local Nusselt numbers along the stator and rotor for different configurations and Reynolds numbers. Pellé and Harmand (2007) performed measurements over the rotor (in the rotor/stator configuration), using a technique based on infrared thermography. A very detailed experimental investigation of the turbulent flow around a single heated rotating disk was performed by Elkins and Eaton (2000).

The flow in the cavity between two disks heated from below (the Rayleigh Bénard convection) with superimposed moderate rotation is used as a model problem for predicting geophysical phenomena (solar and giant planetary convection, deep oceanic convection). The flow with moderate rotation undergoes a series of consecutive bifurcations starting with unstable convection rolls at moderate Rayleigh numbers. The transition culminates at a state dominated by coherent plume structures. The Rayeligh-Bénard convection with superimposed rotation has been studied in rotor/stator cavity among others by Kunnen *et al.* (2005).

In the present paper, we investigate the flow in the rotor/stator cavities of the aspect ratio from the range $L = 3.0$-5.0, curvature parameters $Rm = 1.8$-5.0, using the DNS and LES. The objective of our investigations has been to compute the turbulent heat flux tensor components, the Reynolds stress tensor components, the turbulent Prandtl number and other structural parameters. The obtained data can be useful for heat transfer modeling, but more importantly, such computations can deliver information about the influence of three dimensionality of the mean flow on the turbulence structure. The results are compared to data obtained in experimental investigation of the flow with heat transfer over the heated rotating disk performed by Elkins and Eaton (2000). The present paper results are also compared to the

published data obtained for heated two-dimensional turbulent boundary layers (Wroblewski and Eibeck, 1990; Blair and Bennett, 1987).

The selected Rayleigh-Bénard convection results (with superimposed rotation) are presented in Section 7.

2. Mathematical formulation

We investigate non-isothermal flows in the cavity between stationary and rotating disks of the inner and outer radius R_0 and R_1, respectively. The inter-disks spacing is denoted by $2h$ (Fig. 1). The rotor rotates at a uniform angular

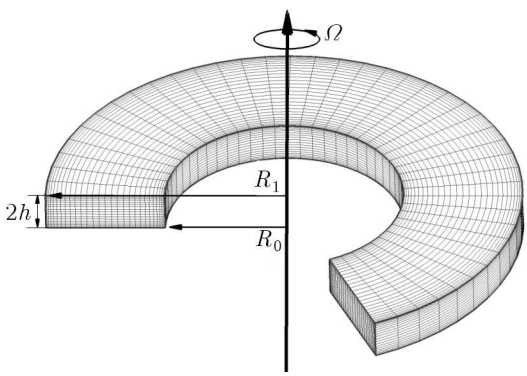

Fig. 1. Schematic picture of computational domain, meridian section

velocity $\Omega = \Omega e_z$, e_z being the unit vector on the axis. The flow is described by the Navier-Stokes, continuity and energy equations, written in a cylindrical coordinate system (R, φ, Z) with respect to the rotating frame of reference

$$\begin{aligned} &\nabla \cdot \boldsymbol{V} = 0 \\ &\rho \frac{\partial \boldsymbol{V}}{\partial t} + \rho(\boldsymbol{V} \cdot \nabla)\boldsymbol{V} + \rho\Omega \times (\Omega \times R) + 2\rho\Omega \times \boldsymbol{V} = -\nabla P + \mu \Delta \boldsymbol{V} - q\rho Z \\ &\frac{\partial T}{\partial t} + (\boldsymbol{V} \cdot \nabla)T = a\Delta T \end{aligned} \tag{2.1}$$

where t is dimensional time, R – radius, P – pressure, ρ – density, $\boldsymbol{V}$ – velocity vector, a – thermal diffusivity and μ is the dynamic viscosity. The flow is governed by the following dimensionless geometrical parameters: aspect ratio $L = (R_1 - R_0)/2h$ and curvature parameter $Rm = (R_1 + R_0)/(R_1 - R_0)$. The dimensionless axial and radial coordinates are: $z = Z/h$, $z \in [-1, 1]$,

$r = (2R-(R_1+R_0))/(R_1-R_0)$, $r \in [-1,1]$. To take into account the buoyancy effects induced by the involved body forces, the Boussinesq approximation is used, i.e. the density associated with the terms of centrifugal and Coriolis forces due to disk rotation, curvilinear motion of the fluid and the Earth acceleration is considered to be variable.

In the paper we consider the flow cases dominated by the centrifugal and Coriolis forces in which the Earth acceleration is negligibly small (the Rayleigh-Bénard convection in which there is a fixed ratio between the rotational and thermal buoyancy is considered only in Section 7). For the flow cases dominated by the rotational buoyancy, the velocity components and time are normalized as follows: ΩR_1, $(\Omega)^{-1}$. The governing parameters are: the Reynolds number $\mathrm{Re} = \Omega R_1^2/\nu$, thermal Rossby number $B = \beta(T_2 - T_1)$, where $\beta = -1/\rho_r(\partial\rho/\partial T)_p$, T_1 and T_2 are two chosen reference temperatures. The dimensionless temperature is defined in the following manner: $\Theta = (T - T_1)/(T_2 - T_1)$. The dimensionless components of the velocity vector in the radial, azimuthal and axial directions are denoted by u, v, w and dimensionless pressure is denoted by p. The no-slip boundary conditions are used with respect to all rigid walls, $u = w = 0$. For the azimuthal velocity component, the boundary conditions are as follows: $v = 0$ on the rotating disk and $v = -(Rm+r)/(Rm+1)$ on the stator. In the paper, we consider the following configuration: the rotating upper disk is attached to the inner cylinder and the heated stator is attached to the outer cylinder. T_1 is the temperature of the upper disk and the inner cylinder, and T_2 is the temperature of the bottom disk and the outer cylinder. The thermal boundary conditions are as follows: $\Theta = 1$ for $z = -1.0$ and for $-1.0 \leqslant r \leqslant 1.0$, $\Theta = 0$ for $z = 1.0$ and for $-1.0 \leqslant r \leqslant 1.0$, $\Theta = 1$ for $r = 1.0$ and for $-1.0 \leqslant z \leqslant 1.0$, $\Theta = 0$ for $r = -1.0$ and for $-1.0 \leqslant z \leqslant 1.0$. This configuration was chosen because is the most unstable. For higher Reynolds numbers, computations are performed only for a section of cavity (for example $0 \leqslant \varphi \leqslant \pi/4$) with the periodicity condition in the azimuthal direction (Fig. 2).

3. Numerical approach

In the LES we use a version of the dynamic Smagorinsky eddy viscosity model proposed by Meneveau *et al.* (1996), in which the required averaging is performed over the fluid particles pathlines, instead of averaging over the direction of statistical homogeneity. The Smagorinsky coefficient is determined by minimizing the modeling error over the pathlines of the fluid particles. The numerical

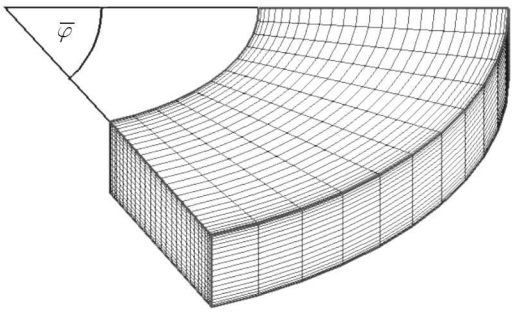

Fig. 2. Section of computational domain

algorithm used for the LES of the non-isothermal flow in the annular cavity, proposed in the papers Tuliszka-Sznitko *et al.* (2008, 2009a,b), is an extended version of the DNS algorithm developed by Serre and Pulicani (2001). The numerical solution is based on a pseudo-spectral Chebyshev-Fourier-Galerkin collocation approximation. In the time approximation we use a second-order semi-implicit scheme, which combines an implicit treatment of the diffusive terms and an explicit Adams-Bashforth extrapolation for the non-linear convective terms. In the non-homogeneous radial and azimuthal directions, Chebyshev polynomials are used with the Gauss-Lobatto distributions to ensure high accuracy of the solution inside the very narrow boundary layers at the disks.

4. Mean flow

For all considered Reynolds numbers $10^5 \leqslant \mathrm{Re} \leqslant 2.5 \cdot 10^5$ the flow exhibits typical Batchelor behavior, which means that the flow consists of two disjoint boundary layers on each disk and of a central inviscid core flow. The flow is pumped radially outward along the rotor and recirculates along the stator. Positive thermal Rossby number $B > 0$ means that the buoyancy-driven secondary flow enforces the basic rotation-driven flow. In the transitional boundary layers, the axisymmetric propagating vortices interpreted as the type II instability and positive spiral vortices interpreted as the type I instability were observed. For higher Re (considered in the present paper) the spiral vortices evolve to more annular vortices.

Figure 3 presents the iso-lines of dimensionless temperature in the meridian section ($Rm = 5$, $L = 5$, $\mathrm{Re} = 10^5$, $B = 0.1$). From Fig. 3 we can see that

the flow is propagated radially outward along the cooled rotor, then it is transported down to the stator along the heated stationary outer cylinder. The flow recirculates along the heated stator and finally is lifted up along the cooled rotating inner cylinder. We observe the largest temperature gradients in the area near to the inner and outer cylinders.

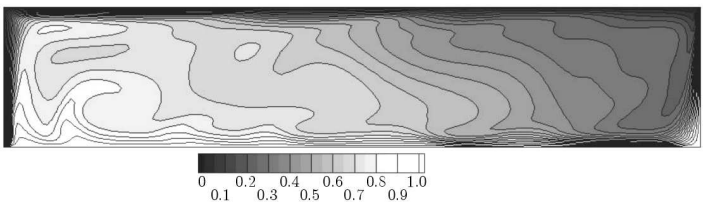

Fig. 3. Iso-lines of temperature; $Rm = 5$, $L = 5$, $\mathrm{Re} = 10^5$, $B = 0.1$

Figure 4 presents the profiles of the mean tangential velocity (computed with respect to the stationary frame of reference) normalized by friction velocity $u_\sigma = [\nu^2((\partial u/\partial z)^2 + (\partial v/\partial z)^2)]^{0.25}$ in terms of $z^+ = u_\sigma z/\nu$. The profiles were obtained in the middle section of the stator boundary layers (cavities of different L, Rm and Reynolds numbers were considered). In Fig. 4, the mean tangential velocity profiles are compared to the conventional logarithmic law of the wall with constants $\kappa = 0.41$ and $C = 5.0$.

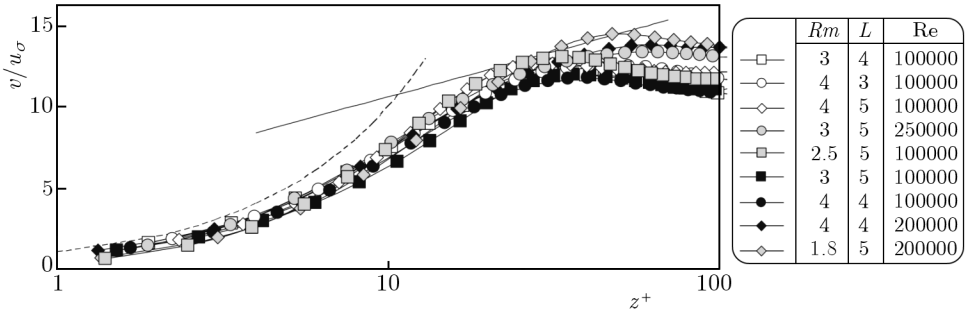

Fig. 4. Mean tangential velocity profiles v/u_σ in terms of z^+. Comparison to the traditional logarithmic law. Profiles obtained in the middle sections of the stator boundary layers

Figures 5a and 5b show mean temperature profiles, $(T_2 - T)/T_\sigma$ in terms of z^+, obtained in the middle section of the stator boundary layers, where T_σ is the friction temperature; $T_\sigma = -\lambda(\partial T/\partial z)/\rho c_p u_\sigma$. The results are compared to the traditional thermal law of the wall with $\kappa = 0.46$ and $C = 3.6$ (Kays and Crawford, 1980). In Fig. 5b, the influence of the Prandtl number on $(T_2 - T)/T_\sigma$ is presented.

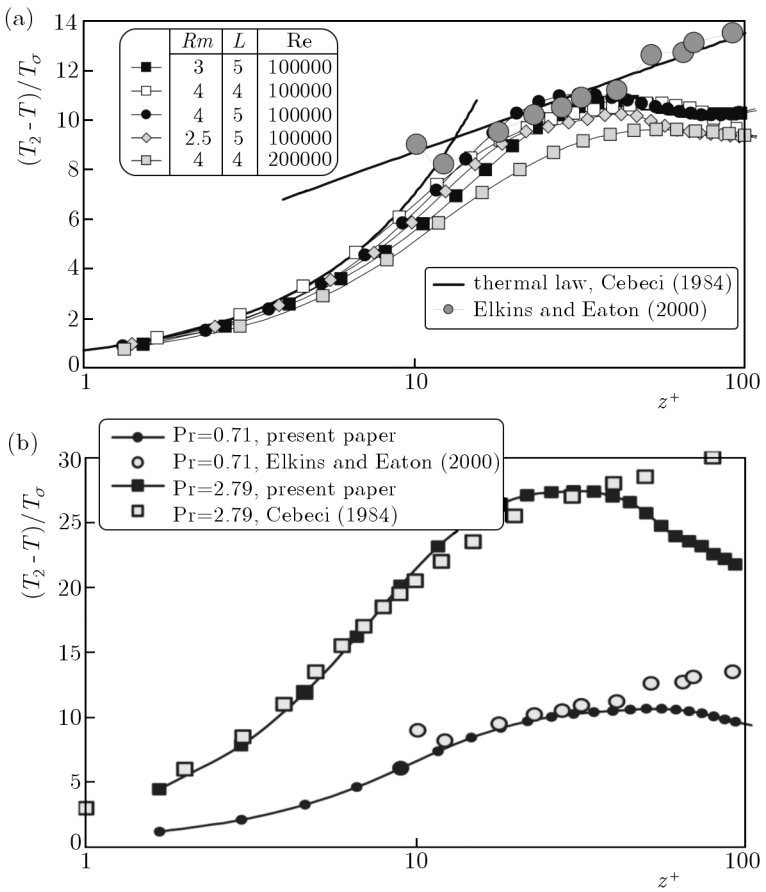

Fig. 5. Distributions of the mean dimensionless temperature $(T_2 - T)/T_\sigma$ in terms of z^+. Stator boundary layers. Middle section of different cavities. (a) $\mathrm{Pr} = 0.71$, (b) $\mathrm{Pr} = 0.71$ and 2.79

5. Turbulent velocity and temperature characteristics

The three main Reynolds stress tensor components obtained in the heated stator and cooled rotor boundary layers, normalized by friction velocity $\sqrt{\overline{u'u'}}/u_\sigma$, $\sqrt{\overline{v'v'}}/u_\sigma$, $\sqrt{\overline{w'w'}}/u_\sigma$ are presented in Fig. 6. We can see strong anisotropy of turbulence in both boundary layers. The turbulence is mostly confined in the stator boundary layer with maximum at the junction between the stator and the stationary outer cylinder. We have found that for the same aspect ratio L and Reynolds number, the Reynolds stress tensor components increase with the decreasing curvature parameter Rm (Fig. 6). Areas of the

most intensive turbulence are also visible in Fig. 7, where iso-lines of the axial velocity component are presented in the section of the whole cavities.

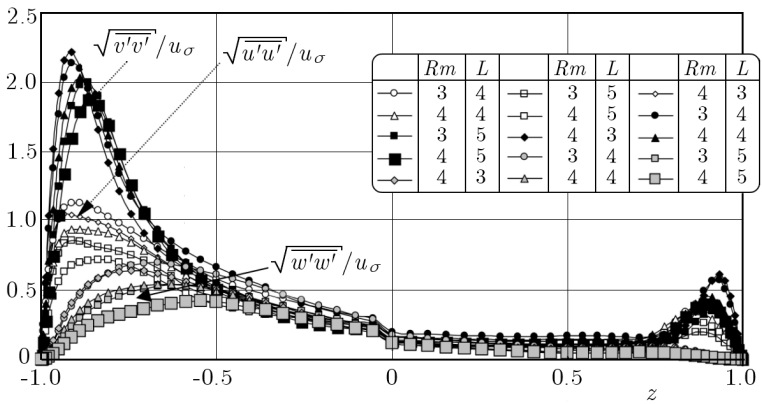

Fig. 6. Reynolds stress tensor components profiles normalized by wall frictions velocity. Results obtained for different L and Rm; $B = 0.1$, $\mathrm{Re} = 10^5$

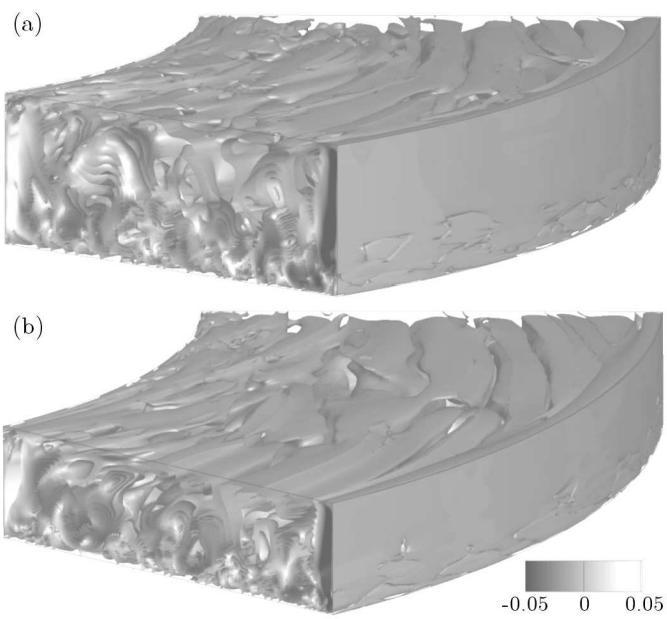

Fig. 7. Iso-lines of the axial velocity component obtained for $Rm = 4$, $\mathrm{Re} = 10^5$, $B = 0.1$ and for different aspect ratios: (a) $L = 3$, (b) $L = 4$

Figure 8 shows the turbulent temperature fluctuations Θ'/T_σ normalized by friction temperature in terms of the axial coordinate normalized by the thickness of the boundary layer z/δ ($\mathrm{Re} = 10^5$). In Fig. 8, the present results are compared to the experimental data obtained by Elkins and Eaton (2000) for the single heated rotating disk (by BC1 and BC2 Elkins and Eaton denoted different thermal adiabatic boundary conditions) and to the results obtained for different two-dimensional boundary layers (Wroblewski and Eibeck, 1990; Blair and Bennett, 1987). For all our computations we obtained the maximum value of Θ'/T_σ at $z/\delta = 0.35$-0.45 whereas Elkins and Eaton (2000) obtained maximum of temperature fluctuations at $z/\delta \sim 0.35$. In the case of two-dimensional boundary layers, Θ'/T_σ equals about 1.7 near the wall and decreases gradually to very small values near the edge of the boundary layer. In Fig. 8, the influence of the Prandtl number on Θ'/T_σ distribution is presented. Numerical simulations have showed that the temperature fluctuations reach maximum approximately at $z^+ \sim 15$ in all considered cases.

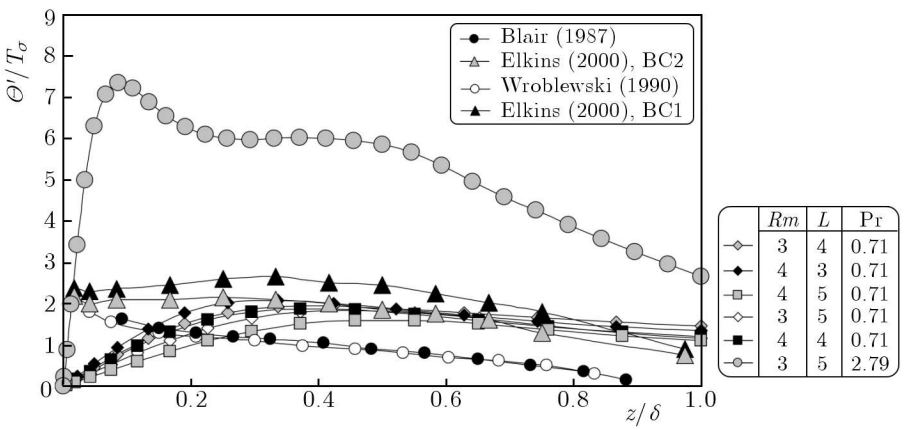

Fig. 8. Distributions of temperature fluctuations Θ'/T_σ normalized by friction temperature in terms of z/δ. $\mathrm{Re} = 10^5$, $B = 0.1$. Middle section of the stator boundary layers. Comparison to the results obtained by different authors for 2D and 3D boundary layers

Figure 9 shows three components of the turbulent heat flux tensor (normalized by the product of friction velocity and friction temperature) versus z/δ. We can see that the largest value was obtained for the component $\overline{v'\Theta'}/u_\sigma T_\sigma$ with the maximum at $z/\delta \sim 0.1$.

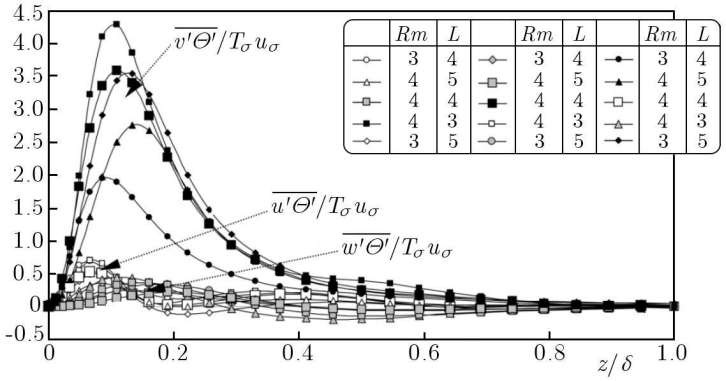

Fig. 9. Turbulent heat flux tensor components profiles obtained in the middle section of the cavity. Stator boundary layers. $\mathrm{Re} = 10^5$, $\mathrm{Pr} = 0.71$

6. Structure parameters

Correlation coefficients and structure parameters are very useful for modeling purposes. The $(\overline{u'^2} + \overline{v'^2})/\overline{w'^2}$ parameter is a measure of the coherence of the turbulent structures. For all analyzed cases, in the stator boundary layer, this parameter reaches a peak near the disk and then decreases rapidly to the value of about 2 near the edge of the boundary layer, showing that the vertical motion is very weak close to the disk. Similarly to other 3D TBLs, the parameter a_1 (defined as the ratio of shear stress vector magnitude to twice the turbulent kinetic energy) obtained in our investigations is reduced significantly below the limit of 0.15 typical for 2D TBL, showing that the boundary layers in rotating cavities are less effective in creating shear stresses from the turbulent motion. The turbulent Prandtl number is defined as the ratio of the eddy diffusivity for momentum to the eddy diffusivity for heat $\mathrm{Pr}_t = (-\overline{w'v'}/\partial\bar{v}/\partial z)/(\overline{w'\Theta'}/\partial\overline{\Theta}/\partial z)$. This is not a strict definition for strongly 3D TBLs, however, we used it to compare our results to the data published in the literature (Elkins and Eaton, 2000). In many 2D TBLs, the turbulent Prandtl number equals 1 in the area near the wall and decreases to 0.8 with increasing z. In Fig. 10, we present Pr_t in terms of z^+. We can see that Pr_t obtained in the present investigations reaches the value of 0.9-1.2 near the wall, then decreases to reach the minimum at $z^+ \sim$ 15-20.

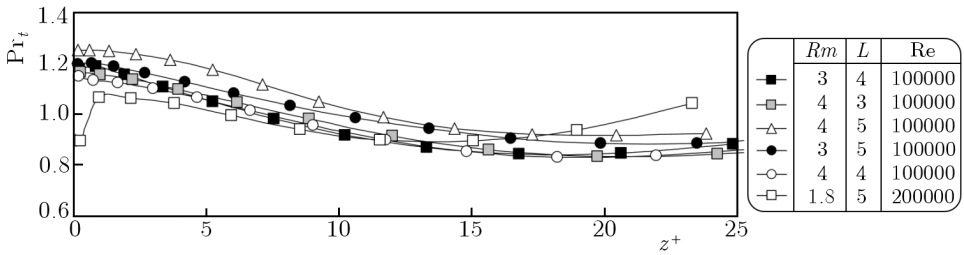

Fig. 10. Turbulent Prandtl number in terms of z^+ obtained in the middle section. Stator boundary layer

7. Rayleigh-Bénerd convection with superimposed rotation

In this Section, we consider the flow between two disks heated from below (from stator) with superimposed moderate rotation. The flow is described by equations (2.1) but the velocity components are normalized with the free-fall velocity $\sqrt{q\beta\Delta T(2h)}$, time is normalized by a convection time scale $2h/\sqrt{q\beta\Delta T(2h)}$ and temperature by $\Delta T = T_2 - T_1$. Length is normalized as in Section 2. The final system of equations received after normalization is presented in Appendix A. We consider the simplest case in which the direction of rotation is aligned with gravity. The dynamics of the rotating Rayleigh-Bénard convection is completely determined by specification of the boundary conditions and by the following governing dimensionless parameters: the Rayleigh number $\mathrm{Ra} = q\beta\Delta T(2h)^3/\nu a$, the Taylor number $\mathrm{Ta} = (2\Omega(2h)^2/\nu)^2$ and the Prandtl number. Boundary conditions are identical as in Section 2 (no-slip boundary conditions are used with respect to all rigid walls, $u = w = 0$, $v = 0$ on the rotating disk and the inner cylinder, and $v = -(Rm + r)/(Rm + 1)$ on the stator and the outer cylinder, isothermal boundary conditions with heated stator and outer cylinder). This paper is not intended to analyze carefully the rotating Bayleigh-Bénard flow properties and statistics. We only would like to demonstrate how significantly different structure of this flow is in comparison to the flow structure analyzed in previous Sections (when the flow was fully dominated by centrifugal and Coriolis forces). With increasing Ra, the flow undergoes a succession of bifurcations before reaching the turbulent state. The first transition is from the static, conducting state, to a convecting flow (in Fig. 11 the iso-lines of the axial velocity component obtained for cavity $\mathrm{Ro} = 0.75$, $\mathrm{Pr} = 0.71$, $L = 5$, $Rm = 1.5$ and different $\mathrm{Ra} = 5 \cdot 10^4$, $2.5 \cdot 10^5$ and $3 \cdot 10^6$ are presented). For the Rayleigh number higher than the critical Ra of the first bifurcation, two-dimensional rolls are observed. In the next

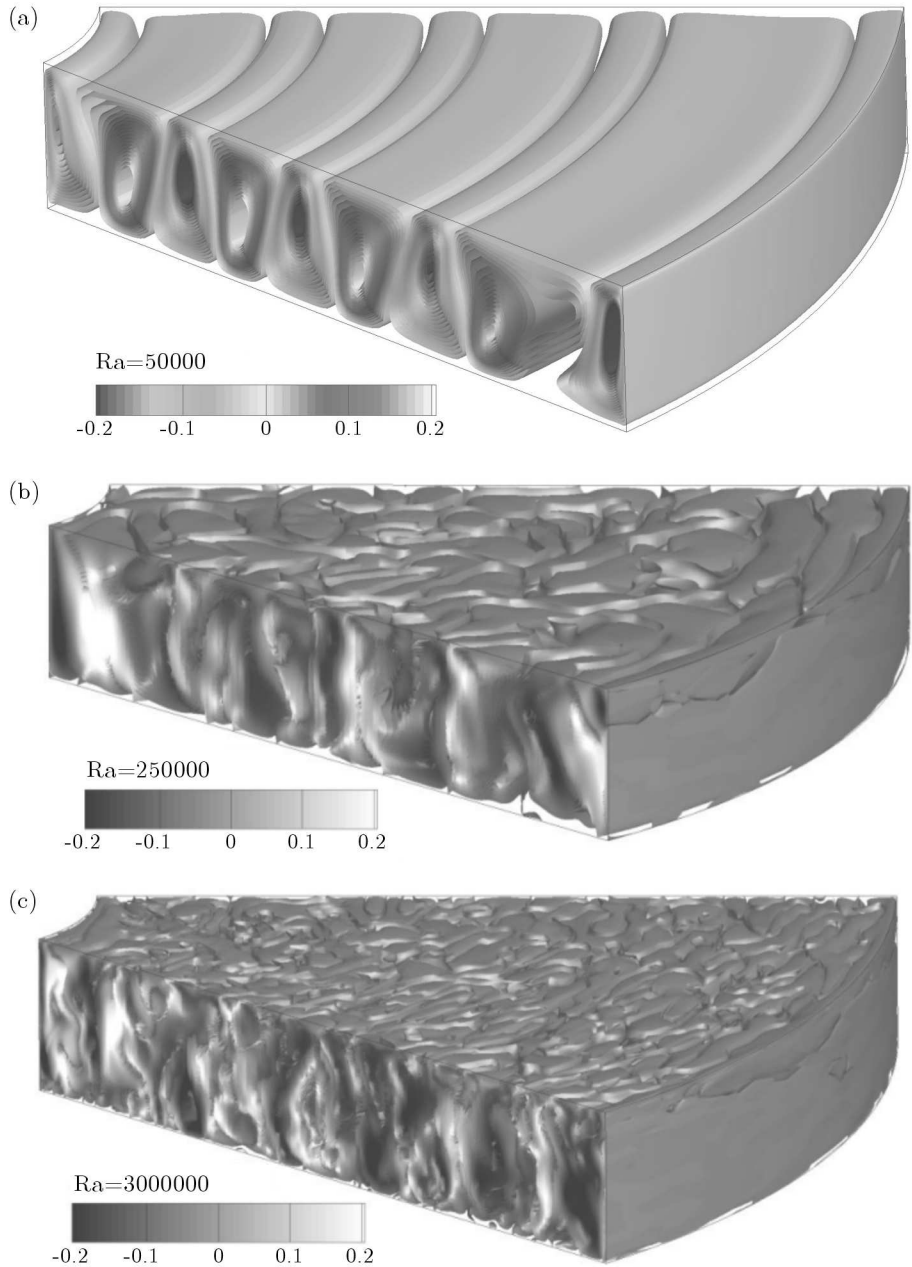

Fig. 11. Iso-lines of the axial velocity component obtained for $L = 5$, $Rm = 1.5$, $\mathrm{Ro} = 0.75$, $\mathrm{Pr} = 1$ and different Rayleigh numbers: (a) $\mathrm{Ra} = 5 \cdot 10^4$, (b) $\mathrm{Ra} = 2.5 \cdot 10^5$, (c) $\mathrm{Ra} = 3 \cdot 10^6$

step the oblique rolls oriented at finite angles appear. As Ra increases further, the periodic convection roll pattern gradually gives way to a state dominated by the chaotic interaction between vertical vortices associated with convection cells. At about $\mathrm{Ra} = 2.5 \cdot 10^5$, coherent structures called plumes appear. We can see that the flow pattern in the rotating Rayleigh-Bénerd convection is significantly different from the flow structures fully dominated by rotation where we observe a one-cell structure.

8. Conclusions

In the paper we presented the Direct Numerical Simulation and Large Eddy Simulation of the non-isothermal transitional and turbulent flow in enclosed cavities of the aspect ratio $L = 3.0$-5.0 and curvature parameters $Rm = 1.8$-5.0 with the heated stator and outer cylinder. The computations have been performed for the thermal Rossby number $B = 0.1$ and for different Reynolds numbers.

The investigated flows belong to the Batchelor family, which means that the flows are divided into two boundary layers separated by a central rotating inviscid core. We have found that the fluid turbulence concentrates in the stator boundary layer and its intensity increases towards the outer cylinder. The instability structures and the level of turbulence depend on the curvature parameter. We focused on the analysis of the three Reynolds stress tensor components and the turbulent heat flux tensor components, which are discussed in the light of experimental results obtained by Elkins and Eaton (2000) for a single rotating disk heated by uniform flux. The obtained distributions of the structural parameter $(\overline{u'^2} + \overline{v'^2})/\overline{w'^2}$ in the stator and rotor boundary layers show that vertical movement near the disks is very weak. The turbulent Prandtl number is analyzed in terms of z^+; Pr_t equals 0.9-1.2 near the wall and decreases almost linearly to the value from the range (0.8-0.9) at $z^+ \sim 15$-20.

A. Appendix

Equations (2.1) after the following normalization: velocity components by the free-fall velocity $\sqrt{q\beta\Delta T(2h)}$, time by the convection time scale $2h/\sqrt{q\beta\Delta T(2h)}$ and temperature by $\Delta T = T_2 - T_1$

$$\frac{1}{L}\frac{\partial u}{\partial r}+\frac{u}{(Rm+r)L}+\frac{1}{(Rm+r)L}\frac{\partial v}{\partial \varphi}+\frac{\partial w}{\partial z}=0 \tag{A.1}$$

$$\begin{aligned}\frac{\partial u}{\partial t}+\frac{u}{L}\frac{\partial u}{\partial r}+\frac{v}{L(Rm+r)}\frac{\partial u}{\partial \varphi}+w\frac{\partial u}{\partial z}-\frac{v^2}{L(Rm+r)}+\sqrt{\frac{\mathrm{PrTa}}{4\mathrm{Ra}}}v\\ +(Rm+r)L\frac{\mathrm{TaPr}}{16\mathrm{Ra}}=-\frac{1}{L}\frac{\partial p}{\partial r}+2\partial\sqrt{\frac{\mathrm{Pr}}{\mathrm{Ra}}}\Big[\frac{1}{L^2}\frac{\partial^2 u}{\partial r^2}+\frac{1}{(Rm+r)L^2}\frac{\partial u}{\partial r}\\ +\frac{1}{(Rm+r)^2L^2}\frac{\partial^2 u}{\partial \varphi^2}+\frac{\partial^2 u}{\partial z^2}-\frac{u}{L^2(Rm+r)^2}-\frac{2}{L^2(Rm+r)^2}\frac{\partial v}{\partial \varphi}\Big]\end{aligned} \tag{A.2}$$

$$\begin{aligned}\frac{\partial v}{\partial t}+\frac{u}{L}\frac{\partial v}{\partial r}+\frac{v}{(Rm+r)L}\frac{\partial v}{\partial \varphi}+w\frac{\partial v}{\partial z}+\frac{uv}{L(Rm+r)}+\sqrt{\frac{\mathrm{TaPr}}{4\mathrm{Ra}}}u\\ =-\frac{1}{(Rm+r)L}\frac{\partial P}{\partial \varphi}+2\sqrt{\frac{\mathrm{Pr}}{\mathrm{Ra}}}\Big[\frac{1}{L^2}\frac{\partial^2 v}{\partial r^2}+\frac{1}{(Rm+r)L^2}\frac{\partial v}{\partial r}\\ +\frac{1}{(Rm+r)^2L^2}\frac{\partial^2 v}{\partial \varphi^2}+\frac{\partial^2 v}{\partial z^2}-\frac{v}{(Rm+r)^2L^2}+\frac{2}{(Rm+r)^2L^2}\frac{\partial u}{\partial \varphi}\Big]\end{aligned} \tag{A.3}$$

$$\begin{aligned}\frac{\partial w}{\partial t}+\frac{u}{L}\frac{\partial w}{\partial r}+\frac{v}{(Rm+r)L}\frac{\partial w}{\partial \varphi}+w\frac{\partial w}{\partial z}=-\frac{\partial P}{\partial z}+\frac{\Theta}{2}\\ +2\sqrt{\frac{\mathrm{Pr}}{\mathrm{Ra}}}\Big[\frac{1}{L^2}\frac{\partial^2 w}{\partial r^2}+\frac{1}{(Rm+r)L^2}\frac{\partial w}{\partial r}+\frac{1}{(Rm+r)^2L^2}\frac{\partial^2 w}{\partial \varphi^2}+\frac{\partial^2 w}{\partial z^2}\Big]\end{aligned} \tag{A.4}$$

$$\begin{aligned}\frac{\partial \Theta}{\partial t}+\frac{u}{L}\frac{\partial \Theta}{\partial r}+\frac{v}{(Rm+r)L}\frac{\partial \Theta}{\partial \varphi}+w\frac{\partial \Theta}{\partial z}\\ =\sqrt{\frac{4}{\mathrm{PrRa}}}\Big[\frac{1}{L^2}\frac{\partial^2 \Theta}{\partial r^2}+\frac{1}{(Rm+r)L^2}\frac{\partial \Theta}{\partial r}+\frac{1}{(Rm+r)^2L^2}\frac{\partial^2 \Theta}{\partial \varphi^2}+\frac{\partial^2 \Theta}{\partial z^2}\Big]\end{aligned} \tag{A.5}$$

References

1. ANDERSSON H.I., LYGREN M., 2006, LES of open rotor-stator flow, *Int. J. Heat Fluid Flow*, **27**, 4, 551-557

2. BLAIR M.F., BENNETT J.C., 1987, Hot-wire measurements of velocity and temperature fluctuations in a heated turbulent boundary layer, *J. Phys. E: Sci. Instrum*, **20**, 209

3. ELKINS C.J., EATON J.K., 2000, Turbulent heat and momentum transport on a rotating disk, *J. Fluid Mech.*, **402**, 225-253

4. GAUTHIER G., GONDRET P., MOISY F., RABAUD M., 2002, Instabilities in the flow between co- and counter-rotating disks, *J. Fluid Mech.*, **473**, 1-21

5. KAYS W.M., CRAWFORD M.E., 1980, *Convective Heat and Mass Transfer*, McGraw-Hill

6. KUNNEN R., GEURTS B., CLERCS H., 2005, Direct numerical simulation of turbulent rotating Rayleigh-Bénard convection, *Direct and Large Eddy Simulation VI*, 233-240

7. LYGREN M., ANDERSSON H.I., 2004, Large eddy simulations of the turbulent flow between a rotating and a stationary disk, *ZAMP*, **55**, 268

8. MENEVEAU C., LUND T.S., CABOT W.H., 1996, A Lagrangian dynamic subgrig-scale model of turbulence, *J. Fluid Mech.*, **319**, 353-385

9. MOISY F., DOARÉ O., PASUTTO T., DAUBE O., RABAUD M., 2004, Experimental and numerical study of the shear layer instability between two counter-rotating disks, *J. Fluid Mech.*, **507**, 175-202

10. PELLÉ J., HARMAND S., 2007, Heat transfer measurements in an opened rotor-stator system air-gap, *Exp. Therm. Fluid Sci.*, **31**, 165-180

11. RANDRIAMAMPIANINA A., BONTOUX P., ROUX B., 1987, Ecoulements induits par la force gravifique dans une cavité cylindrique en rotation, *Int. J. Heat Mass Transfer*, **30**, 7, 1275-1292

12. SERRE E., PULICANI J.P., 2001, A three-dimensional pseudospectral method for rotating flows in a cylinder, *Computers and Fluids*, **30**, 4, 491-510

13. SERRE E., TULISZKA-SZNITKO E., BONTOUX P., 2004, Coupled numerical and theoretical study of the transition flow between a rotating and stationary disk, *Phys. Fluids*, **16**, 3, 688-707

14. SÉVERAC E., SERRE E., 2007, A spectral viscosity LES for the simulation of turbulent flows within rotating cavities, *J. Comp. Phys.*, **226**, 2, 1234-1255

15. TULISZKA-SZNITKO E., SERRE E., BONTOUX P., 2002, On the nature of the boundary layers instabilities in a flow between a rotating and a stationary disc, *C.R. Acad. Sci. Paris II B – Mech.*, **330**, 2, 91-99

16. TULISZKA-SZNITKO E., ZIELINSKI A., 2008, DNS/LES of transitional flow in rotating cavity, *Int. J. Transport Phenomena*, **10**, 3, 223-234

17. TULISZKA-SZNITKO E., ZIELINSKI A., MAJCHROWSKI W., 2009a, LES and DNS of the non-isothermal transitional flow in rotating cavity, *Int. J. Heat and Fluid Flow*, **30**, 3, 534-548

18. TULISZKA-SZNITKO E., ZIELINSKI A., MAJCHROWSKI W., 2009b, Large Eddy Simulation of transitional flows in rotor/stator cavity, *Archives Mech.*, **61**, 2, 93-118

19. Tuliszka-Sznitko E., Zieliński A., Majchrowski W., 2010, LES of the non-isothermal flow in rotating cavity, *Notes on Numerical Fluid Mechanics and Multidisciplinary Design*, **111**, Progress in Hybrid RANS-LES Modelling, ed. Haase, Doerffer, Shia-Hui, Springer-Verlag, 283-292

20. Wroblewski D.E., Eibeck P.A., 1990, An experimental investigation of turbulent heat transport in a boundary layer with an embedded streamwise vortex, PhD Thesis, University of California at Berkeley, Mechanical Engineering Department

Numeryczna symulacja transportu ciepła i pędu w konfiguracjach wirujących

Streszczenie

W artykule przedstawiono wyniki symulacji przepływu (z wymianą ciepła) w obszarze pomiędzy stojanem i wirnikiem oraz dwoma pierścieniami uzyskane z zastosowaniem metod DNS i LES. Badania przeprowadzono dla rozciągłości obszaru $L = 3.0\text{-}5.0$ oraz dla współczynnika krzywizny $R_m = 1.8\text{-}5.0$. Badano struktury niestabilnościowe występujące w warstwie przyściennej wirnika i stojana oraz profile osiowe naprężeń reynoldsowskich, fluktuacji temperatury, turbulentnej liczby Prandtla, profile parametrów strukturalnych i korelacyjnych. Obliczenia przeprowadzono dla różnych liczb Reynoldsa i Prandtla. Uzyskane rozwiązania porównano z wynikami badań eksperymentalnych Elkinsa i Eatona (2000) uzyskanymi podczes badania przepływu wokół pojedynczego wirującego dysku podgrzewanego jednorodnym strumieniem. Rezultaty badań porównywano również z wynikami uzyskanymi dla dwuwymiarowych turbulentnych warstw przyściennych.

Manuscript received December 15, 2010; accepted for print February 28, 2011